PAPER

Zinc coordination to the bapbpy ligand in homogeneous solutions and at liposomes: zinc detection *via* fluorescence enhancement†

Elwin Molenbroek,[a] Natan Straathof,[a] Sebastian Dück,[b] Zahid Rashid,[c] Joop H. van Lenthe,[c] Martin Lutz,[d] Aurore Gandubert,[e] Robertus J. M. Klein Gebbink,[e] Luisa De Cola[b] and Sylvestre Bonnet*[a]

In this work, the complexation of the bapbpy ligand to zinc dichloride is described (bapbpy = 6,6′-bis(2-aminopyridyl)-2,2′-bipyridine). The water-soluble, colorless complex [Zn(bapbpy)Cl]Cl·2H$_2$O (compound **2**·H$_2$O) was synthesized; its X-ray crystal structure shows a mononuclear, pentacoordinated geometry with one chloride ligand in apical position. Upon excitation of its lowest-energy absorption band (375 nm) compound **2** shows intense emission (Φ = 0.50) at 418 nm in aqueous solution, and an excited state lifetime of 5 ns at room temperature. Photophysical measurements, DFT, and TD-DFT calculations prove that emission arises from vibronically coupled Ligand-to-Ligand Charge Transfer singlet excited states, characterized by electron density flowing from the lone pairs of the non-coordinated NH bridges to the π* orbitals of the pyridine rings. Monofunctionalization of the ligand with one long alkyl chain was realized to afford ligand **3**, which can be inserted into dimyristoylphosphatidylglycerol (DMPG) or dimyristoylphosphatidylcholine (DMPC) unilamellar vesicles. For negatively charged DMPG membranes the addition of a zinc salt to the vesicles leads to an enhancement of the fluorescence due to zinc coordination to the membrane-embedded tetrapyridyl ligand. No changes were observed for the zwitterionic DMPC lipids, where binding of the Zn ions does not take place. A modest binding constant was found (5 × 10^6 M^{-1}) for the coordination of zinc cations to bapbpy-functionalized DMPG membranes, which allows for the detection of micromolar zinc concentrations in aqueous solution. The influence of chloride concentration and other transition metal ions on the zinc binding was evaluated, and the potential of liposome-supported metal chelators such as ligand **3** for zinc detection in biological media is discussed.

[a]*Leiden Institute of Chemistry, Gorlaeus Laboratories, Leiden University, P.O. Box 9502, Leiden, 2300 RA, The Netherlands. E-mail: bonnet@chem.leidenuniv.nl; Fax: +31 71 527 44 51; Tel: +31 71 527 42 60*
[b]*CeNTech, University of Muenster, Heisenbergstrasse 11, 48149 Münster, Germany*
[c]*Theoretical Chemistry Group, Debye Institute for Nanomaterials Science, Faculty of Science, Utrecht University, Princetonplein 1, 3584 CC Utrecht, The Netherlands*
[d]*Crystal and Structural Chemistry, Bijvoet Center for Biomolecular Research, Faculty of Science, Utrecht University, Padualaan 8, 3584 CH Utrecht, The Netherlands*
[e]*Organic Chemistry & Catalysis, Debye Institute for Nanomaterials Science, Faculty of Science, Utrecht University, Universiteitsweg 99, 3584 CG Utrecht, The Netherlands*
†Electronic supplementary information (ESI) available. CCDC 863825. For ESI and crystallographic data in CIF or other electronic format see DOI: 10.1039/c2dt32488a

Introduction

Coordination of metal ions to lipid bilayers is an important phenomenon in biological systems, *e.g.* for neural signal transduction or muscle contraction. Typically, monovalent and divalent ions like Na$^+$, K$^+$ or Ca^{2+} bind either to membrane proteins or directly to the phosphate heads of the phospholipids,[1–3] which triggers the opening of ion gates and leakage (pumping) of ions to (from) the cell.[4] Meanwhile, much information has been gathered on the interactions between transition metal ions and lipids bilayers.[5] Earlier work of Reedijk *et al.* investigated the role of metal–lipid interactions in *cis*-platin chemotherapy,[6,7] whereas Constable,[8] Hunter[9,10] and Lehn[11] showed how coordination of transition metal ions to membrane-embedded ligands could induce vesicle aggregation and fusion. It was for example highlighted that when ligands are embedded in the two dimensions of a lipid bilayer their coordination chemistry might be different compared to bulk solution.[9,12] Recent work of Gruber *et al.*[13] has shown how zinc binding to membrane-embedded chelators could quench the fluorescence of amphiphilic dyes self-assembled in the same lipid membrane.

In the last few years we have been interested in the chemistry of the tetradentate 6,6′-bis(2-aminopyridyl)-2,2′-bipyridine

ligand (bapbpy, compound **1**).[14,15] In the first part of this article the synthesis of a zinc(II) complex of the bapbpy ligand, [Zn(bapbpy)Cl]Cl·2H$_2$O (compound **2**·H$_2$O), is reported, as well as its structural, photophysical, and theoretical characterization. We discovered that this water-soluble, colorless compound strongly emits in the blue upon irradiation with near UV light. After fully characterizing the photophysical properties of compound **2** in water we report our investigations on using the bapbpy manifold to detect Zn^{2+} ions in aqueous solutions. The detection of unbound metal ions such as Zn^{2+} (or Cu^{2+}) in neural tissues has developed into a major research field in bioinorganic chemistry due to the clinical relevance of these ions in neurodegenerative diseases such as Alzheimer's disease.[16–20] Robust chemical probes have been developed in the last few years that allow rapid detection of the labile Zn^{2+} pool in living cells. A traditional approach consists in developing water-soluble metal chelators that may be directly taken up by cells, where zinc binding leads to fluorescence enhancement. When the zinc chelator is insoluble in water, which is the case for bapbpy, one may functionalize it with water-solubilizing groups. We used a different approach, *i.e.*, monofunctionalization of the chelator with a lipophilic tail and insertion of the resulting ligand **3** into dimyristoylphosphatidylglycerol (DMPG) or dimyristoylphosphatidylcholine (DMPC) liposomes, to realize zinc sensing at the surface of the vesicles. According to these studies binding of free zinc takes place with anionic DMPG lipids, whereas it does not happen with zwitterionic DMPC lipids. Quantitative fluorescence studies, binding constant measurement, and competitive binding experiments allow us to discuss the potential of such a system for the detection of free Zn^{2+} ions in biological media.[13,18,21–25]

Experimental part

Synthesis

All commercially available chemicals were used as received. 1,2-Dimyristoyl-*sn*-glycero-3-phosphoglycerol (DMPG) and 1,2-dimyristoyl-*sn*-glycero-3-phosphocholine (DMPC) were obtained from Avanti Polar Lipids and stored at −18 °C. Toluene and dioxane were dried under sodium and benzophenone; *N,N*-dimethylformamide was dried under calcium hydride. ^{1}H and ^{13}C NMR was performed on a Bruker DPX300 or AV-400 instrument; chemical shifts are reported in δ (parts per million), and resonances are calibrated to the deuterated solvent peak. All fluorescence intensity measurements were made with an LS-50B luminescence spectrometer (Perkin-Elmer, Beaconsfield, UK) using a quartz cuvette (1.00 cm pathlength) and temperature control (25 °C) by a B. Braun Thermomix 1460. Instrumental parameters and processing data are controlled by the Fluorescence Data Manager software. Unless stated otherwise, excitation and emission wavelengths were set at 363 and 418 nm respectively. UV-visible spectra were performed on a Cary Varian 50 scan UV-Vis spectrometer. LC/MS analysis was done on a JASCO HPLC-system (detection simultaneously at 214 and 254 nm) equipped with an analytical C18

column (4.6 mm D × 250 mm L, 5 μm particle size), in combination with buffers A: H$_2$O, B: MeCN and C: 0.5% aqueous TFA, and coupled to a mass spectrometer with a custom Electro Spray Instrument (ESI). HRMS spectra were recorded with a PE/SCIEX API 165 instrument equipped with an electron spray interface, or a Q-Star Applied Biosystems Q-TOF (TOF-section). Three different buffers were used: buffer A was free of chloride anions and was prepared from KH$_2$PO$_4$ (2.3 mmol), K$_2$HPO$_4$·3H$_2$O (2.6 mmol), and K$_2$SO$_4$ (4.9 mmol) in 500 mL water (phosphate 10 mM pH = 7.0 at 23 °C, I = 50 mM); buffer B was made from KH$_2$PO$_4$ (1.0 mmol), K$_2$HPO$_4$ (1.5 mmol), K$_2$SO$_4$ (9.8 mmol) and KCl (2.5 mmol) in 250 mL water (phosphate 10 mM pH = 7.0 at 23 °C, I = 150 mM, chloride concentration 10 mM), and buffer C from KH$_2$PO$_4$ (1.2 mmol), K$_2$HPO$_4$ (1.3 mmol), K$_2$SO$_4$ (1.6 mmol) and KCl (27.5 mmol) in 250 mL water (phosphate 10 mM pH = 7.0 at 23 °C, I = 150 mM, chloride concentration 110 mM).

6,6′-Dibromo-2,2′-bipyridine was prepared according to a literature procedure.[26] Bapbpy (**1**) was prepared by a modified literature procedure: 6,6′-dibromo-2,2′-bipyridine (2.20 g, 7.02 mmol), S-BINAP (177 mg, 0.290 mmol), Pd$_2$(dba)$_3$ (138 mg, 0.150 mmol) and KO^{t}Bu (5.07 g, 45.0 mmol) were added to a dry, 3-neck round-bottom flask and put under argon. Dry degassed toluene (40 mL) was added, followed by 2-aminopyridine (1.98 g, 21.0 mmol). The reaction mixture was stirred at 80 °C for 3 days. The reaction was allowed to cool to RT and H$_2$O (150 mL) was added. After stirring the mixture for 1 hour the precipitate was filtered and washed with water, diethyl ether, and hexane. The light brown powder was dried by azeotropically removing the water with dry toluene, resulting in 1.70 g of bapbpy (73%). Characterization was identical to the literature.[15]

[Zn(bapbpy)Cl]Cl·H$_2$O (**2**). To a 50 mL round bottom flask, bapbpy (100.0 mg, 0.29 mmol), anhydrous ZnCl$_2$ (36.9 mg, 0.27 mmol) and dry degassed MeOH (25 mL) were added under argon to give a yellow solution. This mixture was stirred overnight. Subsequently the solution was filtered to remove the last traces of bapbpy and evaporated to give a yellow powder. The complex was recrystallized from boiling water and slowly cooled down to 4 °C to obtain pale yellow single crystals of **2**·H$_2$O suitable for X-ray diffraction analysis. Drying the crystals under vacuum afforded compound **2** as a pale yellow solid. Yield: 113 mg (86%). ^{1}H NMR (300 MHz, MeOD) δ 8.07–7.88 (m, 10H), 7.28 (dd, J = 8.2, 5.3 Hz, 4H), 7.09 (td, J = 6.0, 1.1 Hz, 2H) (see Fig. S0†). ^{1}H NMR (D$_2$O, 400 MHz) at 50 °C: δ = 7.47 (t, J = 6.4, 2H), 7.58 (d, J = 8.0, 2H), 7.62 (d, J = 8.8, 2H), 8.22 (m, 4H), 8.31 (t, J = 8.4, 2H), 8.36 (t, J = 8.0, 2H). ^{13}C NMR (300 MHz, MeOD) δ C$_{IV}$: 155.27, 154.51, 147.09, C$_H$: 146.37, 142.12, 141.61, 118.18, 116.17, 115.70, 115.22. ES MS from MeOH solution, m/z (calc.): 467.85 (464.27) [M − 2Cl + 2MeOH]$^{2+}$; 403.77 (402.89) [M − 2Cl$^-$]. ES MS from water +1% HCl, m/z (calc): 475.04 (475.02, [M + H]$^+$); 439.04 (439.04, [M − Cl]$^+$), 341.15 (341.15, [M − Zn-2Cl + H]$^+$), 171.07 (171.08, [M − Zn-2Cl + 2H]$^{2+}$). Elemental Analysis % (calc. for C$_{20}$H$_{16}$Cl$_2$N$_6$Zn·H$_2$O): C: 48.61 (48.56), H: 3.45 (3.67), N: 17.08 (16.99).

3: A mixture of bapbpy (0.15 g, 0.5 mmol), tetrabutyl ammonium bromide (0.15 g, 0.5 mmol) and NaOH powder (0.10 g, 2.5 mmol) was prepared under argon and dissolved in dry dioxane (20 mL). The stirred reaction mixture was heated up to 100 °C (reflux) for 1 hour. Then, lauroyl chloride (0.11 mL, 0.5 mmol) was added dropwise *via* a syringe to the reaction mixture, upon which a colour change from yellow brownish to a dark brownish took place. The reaction mixture was stirred for 4 hours and monitored by TLC (50% EtOAc/petroleum ether, Al_2O_3). After 4 hours it was cooled down to RT and quenched with 1 M HCl to decrease the pH below 2. This mixture was extracted twice with pentane (30 mL). The water layer was basified using solid NaOH to pH > 12. A colour change from green to yellow orange was observed. Then, the aqueous layer was extracted twice with DCM (30 mL). The combined DCM layers were concentrated *in vacuo* to yield the crude product as a yellow brown oil. The crude product was taken up in warm pentane and cooled to RT, followed by a filtration to remove the unreacted bapbpy ligand. The filtrate was concentrated under reduced pressure, and purified by silica column chromatography using a gradient of EtOAc in petroleum ether (5% (v/v) → 20% (v/v) + 1% (v/v) Et_3N, SiO_2). This afforded compound **3** in 59% yield (0.155 g, 0.29 mmol) as a yellow oil. ^1H NMR (400 MHz, DMSO) δ 9.80 (s, 1H, nh), 8.43 (dd, J = 4.8, 1.3 Hz, 1H, l), 8.25 (dd, J = 3.7, 1.2 Hz, 1H, k), 8.22 (d, J = 7.9 Hz, 1H, c), 8.04 (t, J = 7.8 Hz, 1H, b), 7.97–7.88 (m, 2H, h and n), 7.77–7.63 (m, 3H, i, e and f), 7.61 (d, J = 8.2 Hz, 1H, o), 7.49 (dd, J = 18.3, 7.4 Hz, 2H, a and d), 7.34 (dd, J = 7.0, 5.3 Hz, 1H, m), 6.94–6.86 (m, 1H, j), 2.32 (t, J = 7.3 Hz, 2H, α), 1.58 (dd, J = 9.2, 5.0 Hz, 2H, β), 1.31–1.12 (m, 18H, alkyl), 0.81 (t, J = 6.8 Hz, 3H, CH_3). ^{13}C NMR (400 MHz, DMSO) δ 173.19 (C=O), 154.67, 154.40, 154.23, 154.02, 153.94, 152.43 (Cq arom), 148.73, 147.57, 139.51, 138.47, 138.38, 137.71, 122.29, 122.21, 121.56, 118.11, 116.16, 112.59, 112.39, 111.72 (CH arom), 35.70 (CH_2, α), 31.32 (CH_2, β), 29.02, 28.99, 28.84, 28.75, 28.46 (CH_2–CH_2–CH_2–CH_2–CH_2), 24.70 (CH_2), 22.13 (CH_2), 13.99 (CH_3). LC-MS (10–90%B): rt 9.15 min, 523.20 $[M + H]^+$. HR-MS m/z (calc.): 523.31780 (523.31799) $[M + H]^+$. Notations for the assignment of the NMR peaks are given in Fig. S2.†

X-ray crystal structure determination of 2·H₂O

$[C_{20}H_{16}ClN_6Zn]Cl···2H_2O$, Fw = 512.69, pale yellow needle, 0.42 × 0.06 × 0.06 mm³, triclinic, P1̄ (no. 2), a = 7.5685(14), b = 12.3240(15), c = 12.9455(19) Å, $α$ = 114.478(8), $β$ = 96.294(8), $γ$ = 98.286(13)°, V = 1068.1(3) Å³, Z = 2, D_x = 1.594 g cm⁻³, $μ$ = 1.43 mm⁻¹. 11 164 Reflections were measured on a Nonius KappaCCD diffractometer with rotating anode and a graphite monochromator ($λ$ = 0.71073 Å) up to a resolution of $(\sin θ/λ)_{max}$ = 0.61 Å⁻¹ at a temperature of 150(2) K. The crystal appeared to be non-merohedrally twinned with a twofold rotation about uvw = [1,0,0] as twin operation. The twinning was taken into account during integration with Eval14[27] and the refinement was performed on a HKLF-5 type reflection file.[28] The TWINABS program[29] was used for absorption correction and scaling (0.55–0.75 correction range). 3868 Reflections were unique (R_{int} = 0.046), of which 3146 were

observed $[I > 2σ(I)]$. The structure was solved with Direct Methods using the program SIR-97[30] and refined with SHELXL-97[31] against F^2 of all reflections. Non-hydrogen atoms were refined with anisotropic displacement parameters. All hydrogen atoms were located in difference Fourier maps. N–H hydrogen atoms were kept fixed at their located position, O–H hydrogen atoms were refined freely with isotropic displacement parameters, and C–H hydrogen atoms were refined with a riding model. 297 Parameters were refined with no restraints. R_1/wR_2 $[I > 2σ(I)]$: 0.0431/0.0977. R_1/wR_2 [all refl.]: 0.0618/0.1064. S = 1.044. Residual electron density between −0.66 and 0.85 e Å⁻³. Geometry calculations and checking for higher symmetry were performed with the PLATON program.[32]

CCDC 863825 contains the supplementary crystallographic data for this paper.

Theoretical calculations

The geometries of four zinc complexes with different coordination environments, $[Zn(bapbpy)]^{2+}$, $[Zn(bapbpy)Cl]^+$, $[Zn(bapbpy)(OH_2)]^{2+}$, and $[Zn(bapbpy)(OH_2)_2]^{2+}$, were optimised in water with DFT/B3LYP using the 6-31G** basis set for C, H, N, O and Cl, and LANL2TZ for Zn as implemented in the Gaussian 03 suite.[33] The polarizable continuum model (PCM)[34] was used to take into account the bulk solvent effects. The excitation energies of the 30 lowest energy singlet-to-singlet excited states were calculated at the same level of the theory using the PCM(water) model. Electron density difference plots in Fig. 3b and Fig. S11 (ESI†) were realized using NWCHEM[35] and CCP1GUI.[36] In NWCHEM package the Conductor-like Screening Model (COSMO) was used to simulate the solvent effects.[37]

Photophysics

Absorption spectra were measured on a Varian Cary 5000 double-beam UV-Vis-NIR spectrometer and baseline corrected. Steady-state emission spectra were recorded on a HORIBA Jobin-Yvon IBH FL-322 Fluorolog 3 spectrometer equipped with a 450 W xenon-arc lamp, double-grating excitation and emission monochromators (2.1 nm mm⁻¹ dispersion; 1200 grooves per mm), and a Hamamatsu R928 photomultiplier tube. Emission spectra were corrected for source intensity (lamp and grating) by standard correction curves. Time resolved measurements were performed using the time-correlated single-photon counting (TCSPC) option of an Edinburgh LifeSpec II spectrometer. An EPL laserdiode (405 nm; FHWM < 80 ps) with repetition rates between 10 kHz and 1 MHz was used to excite the samples. The excitation sources were mounted directly on the sample chamber at 90° to a double-grating emission monochromator (5.4 nm mm⁻¹ dispersion; 1200 grooves per mm blazed at 500 nm) and collected by an MCP-PMT (Hamamatsu R3809U-50) single-photon-counting detector. The photons collected at the detector are correlated by a time-to-amplitude converter (TAC) to the excitation pulse. Signals were collected using a TCC900 plug-in PC card for TCSPC with START and STOP CFDs, Variable Timing Delay, Time to Amplitude Converter (full range 2.5 ns to 50 μs), Flash

ADC and memory, and data analysis were performed using the commercially available F900 software (Edinburgh Instruments). The quality of the fit was assessed by minimizing the reduced chi squared function (χ^2) and visual inspection of the weighted residuals. All measurements gave a lifetime between 4.9 and 5.0 ns in water in the presence of oxygen. Fluorescence quantum yields were determined using a relative method (reference: 9,10-diphenylanthracene in EtOH, quantum yield 0.88).[38] Luminescence quantum yields (Φ_{em}) were measured in optically dilute solutions (O.D. < 0.1 at excitation wavelength) and compared to the reference emitter by the following equation:

$$\Phi_x = \Phi_r \left[\frac{A_r(\lambda_r)}{A_x(\lambda_x)}\right] \left[\frac{I_r(\lambda_r)}{I_x(\lambda_x)}\right] \left[\frac{n_x^2}{n_r^2}\right] \left[\frac{D_x}{D_r}\right]$$

where A is the absorbance at the excitation wavelength (λ), I is the intensity of the excitation light at the excitation wavelength (λ), n is the refractive index of the solvent, D is the integrated intensity of the luminescence and Φ is the quantum yield. The subscripts r and x refer to the reference and the sample, respectively. All quantum yields were performed at identical excitation wavelengths for the sample and the reference, canceling the $I(\lambda_r)/I(\lambda_x)$ term in the equation.

Vesicle preparation

Aliquots of phospholipids (0.005 mmol) and ligand **3** (0.5–10 mol%, *i.e.*, 0.025 to 0.5 μmol) were mixed from chloroform/MeOH stock solutions and dried under a flow of nitrogen for a few hours. They were subsequently placed under vacuum to remove traces of organic solvents. The lipid mixtures were then hydrated with 3.0 mL of buffer A; the final concentration of the lipids was 1.7 mM. The lipid suspensions were freeze-thawed ten times (from liquid N_2 temperature to +50 °C), and then extruded ten times (at +50 °C) through 200 nm alumina filters (Anotop 10, Whatman). The vesicle-containing samples were conserved in the dark at 4 °C and used within 6 days.

Dynamic light scattering

For each sample the particle size distribution of the vesicles was measured by dynamic light scattering (DLS) using an ALV-5000 multibit multi-tau correlator in combination with a Malvern goniometer and a Spectra Physics argon ion laser operating with vertically polarized light with a wavelength of 824 nm. Typically, a distribution centered between 71 and 95 nm radius was found with a polydispersity index of 0.6.

Zeta potential

Calculation of the zeta potential (ζ) values was made from electrophoretic light scattering experiments, giving the electrophoretic mobility. Analysis was made using the Smoluchowski method. Measurements were performed utilizing a Beckman Coulter Nano C system (Beckman Coulter, Krefeld, Germany). The light source was a laser diode ($\lambda = 658$ nm) with a power of 30 mW. The temperature was kept constant at 298 K during the measurements. Scattered light was detected using a PMT.

The software used for controlling and analysis was a Beckman DelsaNano 2.21 (Beckman Coulter, Krefeld, Germany).

Zinc-binding experiments

For all the fluorescence measurements of the [Zn(bapbpy)Cl]Cl complexes the absorption band at 363 nm was used for excitation. Emission spectra were recorded between 300 and 600 nm at a speed of 200 nm per minute, with the excitation slit set at 5.0 and the emission slit at 0 (the minimum value for the instrument, <2 nm). For a typical measurement, the emission and excitation spectra were recorded first without added zinc and then after the addition of $ZnCl_2$ (each increment was 12.5 μL of a 4×10^{-4} M solution, *i.e.*, 5 nmol of Zn^{2+}). After each addition the solution was mixed, and the emission spectrum measured. For each concentration of ligand **3** in the DMPG membrane, the zinc addition was stopped after the emission intensity remained constant for three consecutive points (see Fig. 4b). These three points were averaged to give I_{sat}, the fluorescence intensity at saturation.

Influence of chloride

LUVs functionalized with ligand **3** (1 mol%) were prepared as above, but using different buffers. For sample A zinc was added as $ZnSO_4$ to the vesicles and buffer A was used. For samples B and C zinc was added as $ZnCl_2$, and buffers B and C were used, respectively.

Binding of other metals

Functionalized LUVs (5 μmol DMPG, 1 mol% of ligand **3**, in 3 mL buffer A) were prepared as above, and then diluted three times with buffer A (final theoretical DMPG concentration: 0.56 mM). For each sample an emission spectrum was taken as a reference. Then, three equivalents (50 nmol) of $TiCl_4$, $VOSO_4 \cdot 5H_2O$, $CrCl_3 \cdot 6H_2O$, $MnCl_2 \cdot 4H_2O$, $FeCl_2 \cdot 4H_2O$, $FeCl_3$, $CoCl_2 \cdot 6H_2O$, $NiCl_2 \cdot 6H_2O$, $CuCl_2$, anhydrous $ZnCl_2$, CdI_2, or Hg-$(OAc)_2$ in water were added (10 μL of a 5 mM solution), and the emission spectrum was measured again. For competition experiments, one equivalent (compared to the first metal) of zinc dichloride was added in the end; a third emission spectrum was measured, and compared to the one with only the first metal.

Results and discussion

Synthesis and X-ray crystal structure

All the compounds investigated are depicted in Scheme 1. The coordination of the bapbpy ligand **1** to zinc(II) dichloride was realized in either dichloromethane or methanol, in dry conditions and at room temperature (see Scheme 1). The resulting pale yellow powder was recrystallized from hot water to afford X-ray quality crystals. Two molecules of water co-crystallize together with a mononuclear pentacoordinated zinc(II) complex. In the crystal of [Zn(bapbpy)Cl]Cl·2H₂O (compound **2·H₂O**), the geometry of the complex is a distorted square pyramid, with the bapbpy ligand coordinated to the basal
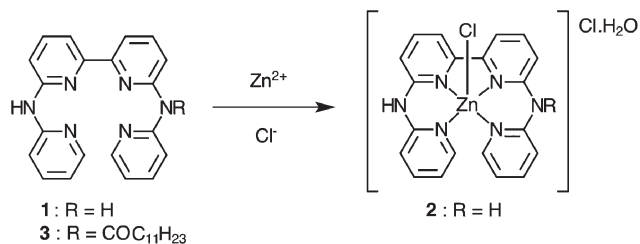
Scheme 1 Structure of ligands **1**, **3**, and of the zinc complex **2**.

Table 1 Selected bond distances (Å) and angles (°) in the crystal structure of compound **2**·H_2O

| Distances		Angles	
Zn1–Cl1	2.2839(10)	Cl1–Zn1–N1	94.51(8)
Zn1–N1	2.095(3)	Cl1–Zn1–N6	105.46(8)
Zn1–N3	2.097(3)	Cl1–Zn1–N3	115.80(8)
Zn1–N4	2.099(3)	Cl1–Zn1–N4	97.10(8)
Zn1–N6	2.086(3)	N4–Zn1–N6	85.26(11)
N2–C5	1.391(4)	N1–Zn1–N3	88.76(11)
N2–C6	1.379(4)	N3–Zn1–N4	77.59(11)
N5–C15	1.376(4)	N1–Zn1–N6	100.85(11)
N5–C16	1.385(5)	N1–N3–N4–N6	−23.54(13)
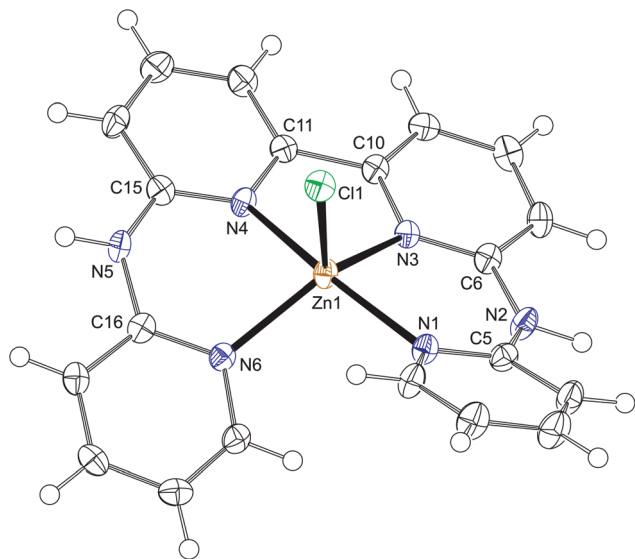
Fig. 1 Displacement ellipsoid plot of the mononuclear cation [Zn(bapbpy)Cl]$^+$ of compound **2**·H_2O, drawn at the 50% probability level. Non-coordinated chloride anion and water molecules have been omitted for clarity.

plane and a chloride anion in the apical position (see Table **1** and Fig. **1**). The unbound chloride counter-anion is involved in hydrogen bonding between the lattice water molecules and one of the uncoordinated N–H bridges of the bapbpy ligand. The two water molecules are not equivalent, one being hydrogen-bonded to the second N–H bridge, and the other water molecule to two chloride anions. According to elemental analysis one of these water molecules is removed when the crystals are crushed and dried under vacuum at 60 °C. The resulting powder, compound **2**, has the chemical formula [Zn(bapbpy)-Cl]Cl·H_2O.

The very high fluorescent quantum yield of compound **2** in water (see below) opened up the possibility to use the bapbpy manifold for the detection of free Zn^{2+} ions *via* fluorescence enhancement. As bapbpy itself is insoluble in water its functionalization with a long lipophilic tail was investigated in order to increase its solubility in lipid bilayers and finally obtain water solubility of the metal chelator using liposomes.[5] Mono-acylation of the NH bridges of ligand **1** was realized using one equivalent of lauroyl chloride and statistical reaction conditions (Scheme 2). Due to the electron-withdrawing properties, and possibly to the steric bulk, of the pyridyl groups, the nucleophilicity of the secondary amines of ligand **1** is low. Following a series of unsuccessful and low-yielding experiments using NaOH or NaH in DMF or DMSO we finally adopted a method published by Ogawa *et al.* using tetrabutyl ammonium bromide as additive and dioxane as the solvent.[39] Thus, preliminary deprotonation in hot dioxane with excess NaOH in the presence of *n*-Bu$_4$NBr, followed by the addition of one equivalent of lauroyl chloride, afforded compound **3** in proportions higher than 50% according to LC-MS of the crude product (see Fig. S1†). In such conditions, the disubstituted compound **3′** (Scheme 2) was only observed in trace amounts. Acid–base washing, pentane extraction of the solid, and silica gel column chromatography allowed for isolating the pure monofunctionalized ligand **3** with a preparative yield of 59%.

LC-MS analysis, ^{1}H NMR spectroscopy and high-resolution mass spectroscopy unambiguously conclude to the dissymmetric nature of ligand **3**. First, LC-MS analysis of the purified product neither shows the peak of the starting bapbpy ligand **1** at 4.06 min nor that of the diacylated compound **3′** at 9.47 min (see Fig. S1b†). Second, in the ^{1}H NMR spectrum of **3** the ratio between the intensity of the triplet of the COCH$_2$ protons of the side chain and that of the bridging NH is two. Third, high-resolution mass spectrometry shows a peak at *m/z* = 523.3178 expected for [**3** + H]$^+$ (calc. 523.3185), and no peak around 705.5 for [**3′** + H]$^+$ (see Fig. S1b†). Finally, 2D COSY (Fig. S2†)
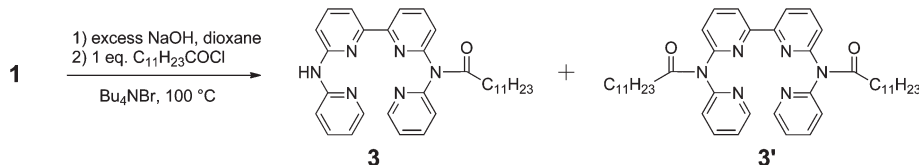
Scheme 2 Monoacylation of the bapbpy ligand **1**.
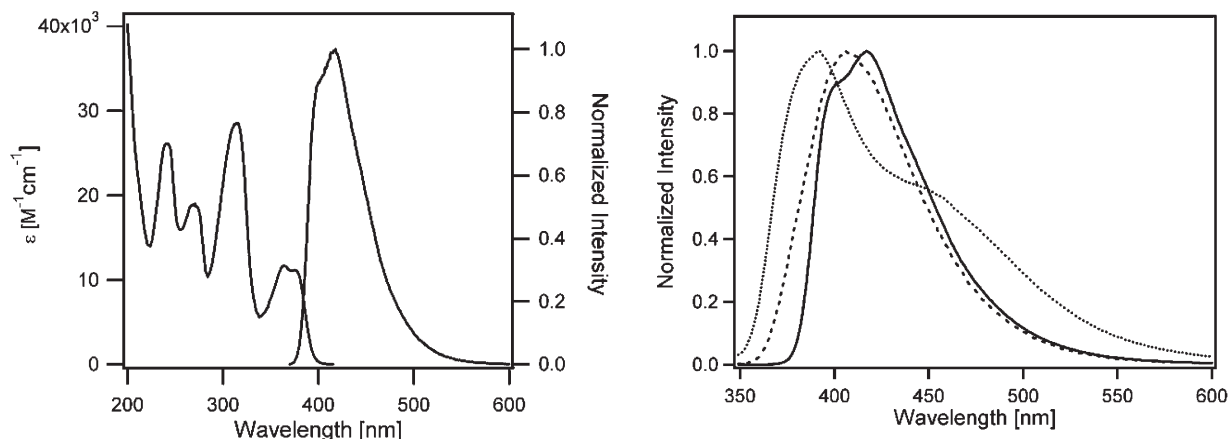
Fig. 2 Left: absorption and emission spectra of **2** in water; right: emission of **2** in water (solid), THF (dotted), and DMF (dashed) at room temperature. Excitation: 312 nm.

and NOESY correlation NMR experiments clearly distinguished the expected four non-equivalent pyridyl rings of the dissymmetric product, which concluded to the nature of **3**.

Photophysical properties

Absorption and excitation spectra of the Zn complex **2** and of the ligands **1** and **3** in DMF solution are displayed in the ESI (Fig. S3 and S4†). The absorption of **2** in water is depicted in Fig. 2 (left). The spectra show intense π–π* transitions in the UV region and a less intense band at about 364 nm which can be assigned as an intraligand charge-transfer (^{1}CT) band since the absorption in a less polar solvent (THF) shows a strong decrease in intensity and a shift (see Fig. S5†). All the compounds emit in DMF solution in the 400–430 nm region (see Table 3, Fig. S6†). Although the bapbpy ligand **1** only dissolves

in DMF or DMSO, compound **2** is soluble in water, where it emits under normal daylight a blue glow that can be seen with the naked eye. The emission spectrum of **2** in water is shown in Fig. 2 (left). It displays a broad structureless emission with a maximum at 418 nm upon excitation at 375 nm. A significant emission quantum yield of 0.50 and an excited state lifetime of 5.0 ns were found for **2** in water at 25 °C (see Table 2). The data are supportive of emission from a singlet ligand-centered state with a charge transfer (CT) character for compound **2**. Indeed decreasing the polarity of the solvent from water to DMF to THF leads to a shift at higher energy of the emission (Fig. 2, right). A further proof of the CT character of the emission comes from the emission in a solid matrix (MeOH–EtOH, 4 : 1, see Fig. S7 and S8†). At 77 K the emission spectrum of **2** shows clear vibronic coupling as expected for a ligand-centered transition and a double exponential decay of 3.4 and 6.5 ns. Similar vibronic coupling and biexponential behaviour are observed for compounds **1** and **3** at low temperature (see Table 3 and Fig. S8†). To evaluate any possible aggregation with increasing concentration the emission intensity at 440 nm was measured for several solutions within a wide range of concentrations (1.1×10^{-3} mol L^{-1} to 2.1×10^{-5} mol L^{-1}, see Fig. S9†). The emission intensity increases proportionally with the concentration of **2**, which accounts for the absence of quenching in bulk solution

Table 2 Photophysical properties of compound **2** in water

Compound	$\lambda_{abs}{}^a$ [nm] ($\varepsilon \times 10^{-3}$/ [M^{-1} cm^{-1}])	λ_{em} RT^a [nm]	φ^b	$\tau_{rt}{}^c$ [ns]
2	241 (26), 269 (19), 316 (29), 364 (11.7)	401 (sh), 418	0.50	5.0

^{a} Excitation: 312 nm. ^{b} Quantum yield was measured using the relative method (reference: 9,10-diphenylanthracene in ethanol[38]). ^{c} Monitored at λ_{em} = 440 nm.

Table 3 Photophysical properties of compounds **1**, **2** and **3** in organic solvents

Compound	$\lambda_{abs}{}^{a,b}$ [nm] ($\varepsilon \times 0^{-3}$/ [M^{-1} cm^{-1}])	λ_{em} RT^{a,c} [nm]	$\varphi_{rt}{}^{a,e}$	$\tau_{rt}{}^{a,f}$ [ns]	λ_{em} 77 K^d [nm]	$\tau_{77\,K}{}^{d,f}$ [ns]
1	278 (8.7), 301 (5.7), 340 (4.3)	404	0.35	5.34	373, 389	0.9 ns (78%), 5.3 ns (22%)
2	278 (25), 302 (18), 343 (11.5), 391 (2.6, sh)	406	0.35	5.27	396, 418, 443	3.4 ns (24.9%) 6.5 ns (75.1%)
3	279 (23), 303 (16, sh), 338 (8.9)	424	0.55	12.13	391	2.4 ns (16.5%) 10.4 ns (83.5%)

^{a} In DMF. ^{b} 'sh' denotes a shoulder. ^{c} Excitation: 312 nm. ^{d} In MeOH–EtOH (1 : 4) matrix. ^{e} Quantum yields were measured using the relative method (reference: 9,10-diphenylanthracene). ^{f} Monitored at λ_{em} = 420 nm.

Table 4 Selected distances (Å) and angles (°) in the theoretical structure of [Zn(bapbpy)Cl]⁺ minimized by DFT/B3LYP in PCM(water)

Distances		Angles	
Zn1–Cl1	2.380	Cl1–Zn1–N1	98.1
Zn1–N1	2.152	Cl1–Zn1–N6	109.7
Zn1–N3	2.168	Cl1–Zn1–N3	117.1
Zn1–N4	2.148	Cl1–Zn1–N4	98.1
Zn1–N6	2.179	N4–Zn1–N6	82.7
N2–C5	1.386	N1–Zn1–N3	85.8
N2–C6	1.383	N3–Zn1–N4	76.3
N5–C15	1.386	N1–Zn1–N6	100.7
N5–C16	1.393	N1–N3–N4–N6	24.9

at the concentrations that were later on used for aggregate formation (see below). All the photophysical data are summarized in Tables 2 and 3.

Theoretical calculation

DFT and TD-DFT calculations were undertaken to study the excited states leading to the emission of compound **2**. The influence of the coordination environment of zinc on the excited states of the complex was in a first step investigated by DFT/B3LYP energy minimization using the 6-31G** basis set for C, H, N, O and Cl, and LANL2TZ for Zn as implemented in Gaussian 03.[33] The polarizable continuum model, PCM-(water),[34] was used in these calculations to simulate solvent effects. Four different species potentially present in aqueous solution were minimized, first in the vacuum and then in water, including [Zn(bapbpy)Cl]⁺, [Zn(bapbpy)]²⁺, [Zn(bapbpy)-(OH₂)]²⁺, and [Zn(bapbpy)(OH₂)₂]²⁺. The Hessian calculations in water confirmed that the geometries for all four species are local minima as no imaginary frequencies were found for any species. PDB files containing the coordinates of the four minimized species can be found in the ESI.† Selected distances and angles for the DFT-minimized structure of [Zn(bapbpy)-Cl]⁺ are given in Table 4; they match well with that observed in the crystal structure of compound **2·H₂O** (see Table 1).

The energies of the transitions to the 30 lowest energy singlet-to-singlet excited states were calculated for these four species using TD-DFT/B3LYP and PCM(water) as implemented in Gaussian 03.[33] Under this level of approximation neither the nature of the ancillary ligands (Cl⁻ or OH₂) nor the coordination geometry (four-, five- or six-coordinate) had a clear influence on the calculated spectrum (see Fig. S10†). As a consequence, we only discuss in the following further results obtained with [Zn(bapbpy)Cl]⁺.

Table 5 shows the calculated transition energies and oscillator strengths of the most intense singlet-to-singlet transitions ($f > 0.05$) for [Zn(bapbpy)Cl]⁺ in water (see also Fig. S10†). Only one intense singlet-to-singlet transition was found above 360 nm that would account for the resolved doublet experimentally observed at 364 and 375 nm. Considering the vibronic structure clearly observed in the emission spectrum of **2** at 77 K the low-energy doublet in the electronic absorption spectrum might be due to vibronic coupling as well. Following a method suggested by Ciofini et al.,[40] ground-

Table 5 Energies and oscillator strengths for the main singlet-to-singlet transitions ($f > 0.05$), as calculated by TD-DFT/B3LYP for [Zn(bapbpy)Cl]⁺ in PCM-(water)

Roots (singlets)	Energy (eV)	Energy (nm)	Oscillator strength f
1	3.37	368	0.235
3	4.03	307	0.067
4	4.10	302	0.186
5	4.33	286	0.074
6	4.38	283	0.084
7	4.47	277	0.449
8	4.58	270	0.052
10	4.77	260[a]	0.077
11	4.77	260[a]	0.067
13	4.88	254	0.103
14	4.92	252	0.154
15	5.17	240	0.071
16	5.22	237	0.090

[a] The energies of roots 10 (260.110 nm) and 11 (259.729 nm) are rounded off to 260 nm.
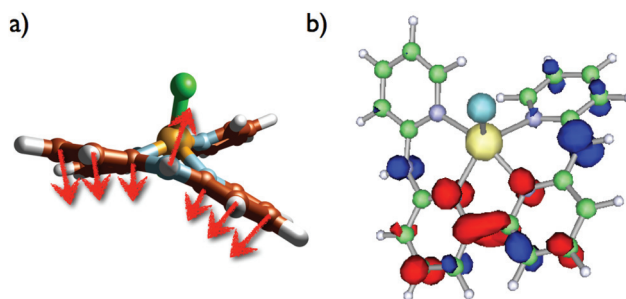
Fig. 3 (a) Third normal mode for [Zn(bapbpy)Cl]⁺ in water according to DFT/B3LYP calculations using PCM in water (calculated energy: 44.4 cm⁻¹). (b) Electron density difference plots for the first singlet-to-singlet electronic transition of [Zn(bapbpy)Cl]⁺ according to TD-DFT/B3LYP calculations in water using COSMO (calculated energy: 365 nm). Blue lobes correspond to a region of depleted electron density in the excited state, and red lobes to increased electron density in the excited state.

state vibrations in the solvent were first calculated using PCM-(water),[34] which showed that [Zn(bapbpy)Cl]⁺ has many normal modes at energies below 100 cm⁻¹ that might be thermally populated at room temperature. One of these low normal modes, i.e. the third lowest mode, calculated at 44.4 cm⁻¹, is for example represented in Fig. 3a. It corresponds to a "butterfly"-type motion around the non-coordinated amine bridges. An electron density difference plot was also made for the lowest-energy transition of [Zn(bapbpy)Cl]⁺ (see Fig. 3b and S11†), which shows that it is a ligand-centered, π–π* transition with strong contributions of the nitrogen p orbitals of the same non-coordinated amine bridges. Qualitatively, these NH bridges are thus involved both in the transitions to the lowest singlet state, and in low-energy, ground-state vibrations of the complex, which are susceptible of being thermally populated at room temperature. Overall, these theoretical calculations support the hypothesis that the resolved doublet observed in the UV-Vis spectrum of compound **2** is due to vibronic coupling.
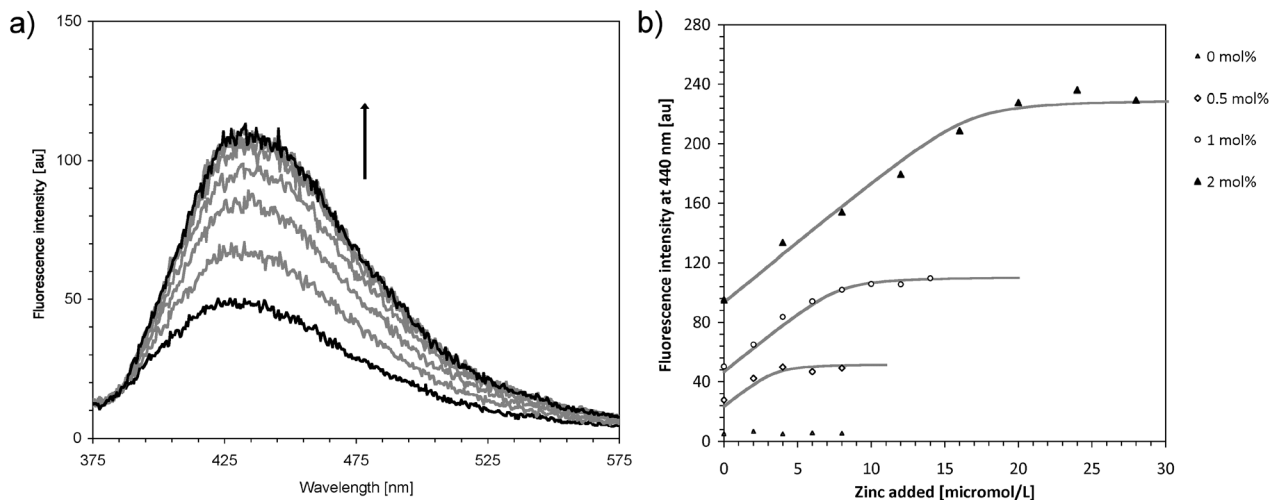
Fig. 4 (a) Evolution of the fluorescence spectrum of DMPG vesicles containing 1 mol% of ligand **3** upon addition of zinc dichloride (0, 5, 10, 15, 20, 25, 30 and 35 nmol, corresponding to 0, 0.1, 0.2, 0.3, 0.4, 0.5, 0.6 and 0.7 equivalent, respectively). (b) Evolution of the fluorescence intensity at 440 nm upon addition of zinc dichloride, with different concentrations of ligand **3** in DMPG membranes (0, 0.5, 1, and 2 mol%). Solid curves show modeling with a binding constant K_a of 5×10^6 M^{-1} (see ESI†). Conditions: LUV, lipid concentration 1.7 mM, bulk concentrations in **3** are 8.33, 16.7, and 33.3 μM for 0.5, 1, and 2 mol%, respectively; $T = 25$ °C, 10 mM phosphate buffer pH = 7.0, total ionic strength 50 mM. [au] = arbitrary units. See also Fig. S14† for the fluorescence response vs. Zn^{2+} concentration expressed in equivalent of ligand **3**.

Vesicle preparation and the influence of the lipid charge on zinc(II) binding to the membrane

Large unilamellar vesicles (LUVs) made of either 1,2-dimyristoyl-*sn*-glycero-3-phosphorylcholine (DMPC) or 1,2-dimyristoyl-*sn*-glycero-3-phosphorylglycerol Na$^+$ salt (DMPG) lipids and x = 0.5–10 mol% of ligand **3** were prepared as described in the Experimental part. The lipid vesicles appear here as a means to solubilize in water the highly lipophilic zinc chelator **3**. The size distribution of the vesicles was measured by dynamic light scattering; they were centered between 71 and 95 nm radius depending on the sample, with an average radius of 86 nm. Each sample was found to be moderately fluorescent due to the embedding of the polypyridyl ligand within the bilayer.

In a second step, one equivalent of zinc dichloride (compared to the amount of ligand **3**) was added to the vesicles, and the fluorescence of the solution was measured again. For DMPC samples, the fluorescence did not vary appreciably after several hours at room temperature (see Fig. S12†). By contrast, the fluorescence for the DMPG sample increased significantly within mixing times, and the wavelength maximum of the fluorescence spectrum of ligand **3** in DMPG membrane, situated at 430 nm, was slightly shifted to 440 nm after zinc addition (see Fig. S12†). With 1 mol% of ligand **3** in the membrane, bi-exponential fluorescence lifetimes were measured: from 1.4 ns (47.8%) and 8.6 ns (52.2%) before zinc addition. They slightly changed after zinc coordination: 1.88 ns (29.3%) and 4.5 ns (70.7%). Finally, in those samples the zeta potential also became less negative, from −51.06 mV to −27.07 mV, after zinc addition.

These results account for fast coordination of zinc, at room temperature, to the bapbpy manifold of ligand **3** embedded in the anionic DMPG bilayer. They also clearly show the critical influence of the lipid charge on the coordination chemistry between the free zinc(II) ions and the bilayer-embedded neutral ligand. The reason for such a different coordination behavior is still unclear, although electrostatic forces play an obvious role. One possibility is that the ligand may adopt a "wrong" conformation in zwitterionic membranes, *e.g.*, it might be buried in the hydrophobic layer where the zinc ions cannot go. Alternatively, the positive charge of the ammonium heads of DMPC might create a repulsive energy barrier that hampers coordination. Another hypothesis is that electrostatic forces would first drive the exchange of bulk Zn^{2+} cations with the counter-cations of the DMPG lipids, and that in a second step the Zn^{2+} cations "adsorbed" at the membrane would meet and coordinate ligand **3** by 2D diffusion at the liposome surface. It has been suggested that host–guest interactions may become up to 1000 times more likely when they take place in 2D, as opposed to the same interaction in a 3-dimensional space.[12,41] Although the interactions between negatively charged lipids and metal cations have been studied extensively,[42,6,43,44] the present study represent a demonstration that lipid charges are an important parameter in the building of a liposomal platform for sensing a metal ion in aqueous solution.

Fluorescent studies with DMPG vesicles

In order to quantitatively measure zinc(II) binding at the membrane-embedded ligand the effect of increasing amounts of zinc dichloride on the fluorescence intensity of DMPG vesicles functionalized with ligand **3** was measured (see Fig. 4 for 0.5, 1, and 2 mol%, and Fig. S13a† for 5 and 10 mol%). Since the emission quantum yield cannot be measured in water due to the low solubility of the compound, and since we cannot

estimate it in the vesicles due to the scattering of the medium, we neglected the initial emission. We believe that the emission quantum yield is much lower in the lipid layer than in the pure organic solvent. From the initial intensity I_0 in the absence of Zn^{2+}, the fluorescence of each sample increased until a plateau was reached (intensity I_{sat}). A good linearity of the fluorescent response to zinc binding was obtained even at a high ligand concentration (Fig. S13a†), where significant filtering of the fluorescence intensity by the concentrated solutions took place (see Fig. S13b†). At such high concentrations, we cannot fully exclude that two ligands **3** bind to the same zinc ion to produce a more flexible, less fluorescent species,[9] which might also contribute to the lowering of the fluorescent response. For a ligand concentration in the membrane of 1 mol%, the maximum fluorescence increase $(I_{sat} - I_0)/I_0$ was found to be 113%. The variations of the fluorescence intensity as a function of the added zinc concentration for different amounts of ligand **3** in the DMPG bilayer were modeled by assuming a 1:1 binding scheme where Zn^{2+} cations are unable to cross the membrane; a binding constant K_a of $\sim 5 \times 10^6$ M^{-1} was obtained (see Fig. 4b and ESI†). Such a value allows for detecting free zinc ions in the micromolar range or above.

Influence of chloride anions

Biological media contain chloride anions, and in order to check the potential of our system for *in vitro* detection of free zinc the behavior of DMPG-embedded ligand **3** in the presence of varying concentrations of chloride anions was studied. In the solid state one chloride anion was bound to the zinc complex, but in solution the Zn–Cl bond might be hydrolyzed, which might influence the fluorescence intensity of the complex. Three types of samples containing 1 mol% of ligand **3** in DMPG vesicles were prepared: sample A contained no chloride anions in the buffer, Zn^{2+} being added as zinc sulfate (chloride-free conditions); samples B and C contained chloride concentrations of 10 and 110 mM in the buffer, respectively, which is close to the typical concentrations found in the cytoplasm and extracellular space, respectively. For both samples B and C zinc was added as zinc dichloride. As can be seen in Fig. 5, the evolution of the fluorescence intensity with gradual addition of zinc(II) for samples A, B and C follows the general trend presented in Fig. 4b, with a slightly reduced (−15%) saturation intensity for chloride-free sample A. Most importantly, samples B and C behaved very similarly, which points to the similar response of the fluorescence when the functionalized DMPG vesicles are inside or outside a cell.

## Coordination of first-row transition metal ions and competition experiments

The behavior of ligand **3** embedded in DMPG membranes was studied as a function of the nature of the metal added to the sample (see Fig. 6a). Thus, Ti^{4+}, V^{4+}, Cr^{3+}, Mn^{2+}, Fe^{2+}, Fe^{3+}, Co^{2+}, Ni^{2+}, Cu^{2+}, Zn^{2+}, Cd^{2+} and Hg^{2+} were added to eleven DMPG samples containing 1 mol% of ligand **3**, and the variation of fluorescent intensity recorded after the addition of the
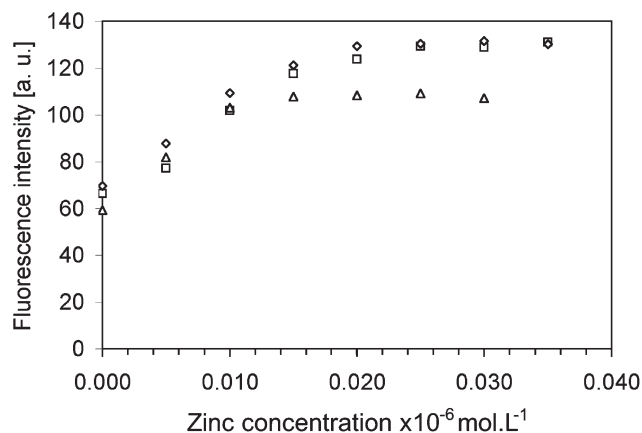
Fig. 5 Variation of fluorescence intensity of DMPG vesicles loaded with 1 mol% of ligand **3** with varying amounts of zinc(II), as a function of chloride concentration. Triangles: no chloride (total ionic strength 50 mM, see text); squares: $[Cl^-]$ = 10 mM (sample B, total ionic strength 150 mM); diamonds: $[Cl^-]$ = 110 mM (sample C, total ionic strength 150 mM). Conditions: LUV, lipid concentration 1.7 mM, 25 °C, 10 mM phosphate buffer pH = 7.0.

metal. In each case three equivalents of the metal ion were added compared to the amount of ligand present in the membrane in order to ensure saturation of the fluorescence intensity. It was indeed assumed that the saturation behavior observed with Zn^{2+} (see above) due to coordination of the metal ion to ligand **3** may be generalized to other metal ions. Overall, a fluorescence *increase* was only observed for Zn^{2+} and Cd^{2+}, whereas for all other metals a fluorescence *decrease* was observed, with the highest variation observed for Ni^{2+}, Cu^{2+} and Hg^{2+}. In all these experiments, the highest variations in fluorescence intensity, whether positive or negative, were $\sim 50\%$ (*i.e.*, $I_{sat}/I_0 = 1.5$).

This behavior is peculiar for metal sensing, as most zinc-detecting chelators described in the literature usually show similar fluorescence intensities of the sensor in the presence and in the absence of metal ions other than Zn^{2+} (or Cd^{2+}). In other words, a low response is usually observed for metal ions with unfilled d orbitals.[17,18] In the case of compound **3** at DMPG liposomes, we assume that the excited state responsible for fluorescence, like for bapbpy, is an LLCT state involving the non-coordinated NH bridge. A possible explanation for fluorescence quenching is an efficient electron transfer from the amino group to the metal ion. Such a mechanism cannot occur in the free ligand or when **3** is coordinated to non-redox active ions such as Zn^{2+}, but it does take place when one or several d-orbitals of the chelated metal are empty. For many donor–acceptor zinc sensors[45] the electronic effects of Zn^{2+} binding result in changes in the HOMO and LUMO energies of the ligand. In the case of ligands **1** and **3** the HOMO–LUMO gap does not change significantly upon binding to the metal. Most probably, the higher quantum yield of the LLCT-based emission after zinc coordination arises from the more rigid structure of the ligand once coordinated to the metal center, whereas before coordination the tetradentate ligand stays in a highly flexible, extended conformation typical of bipyridine chelates.
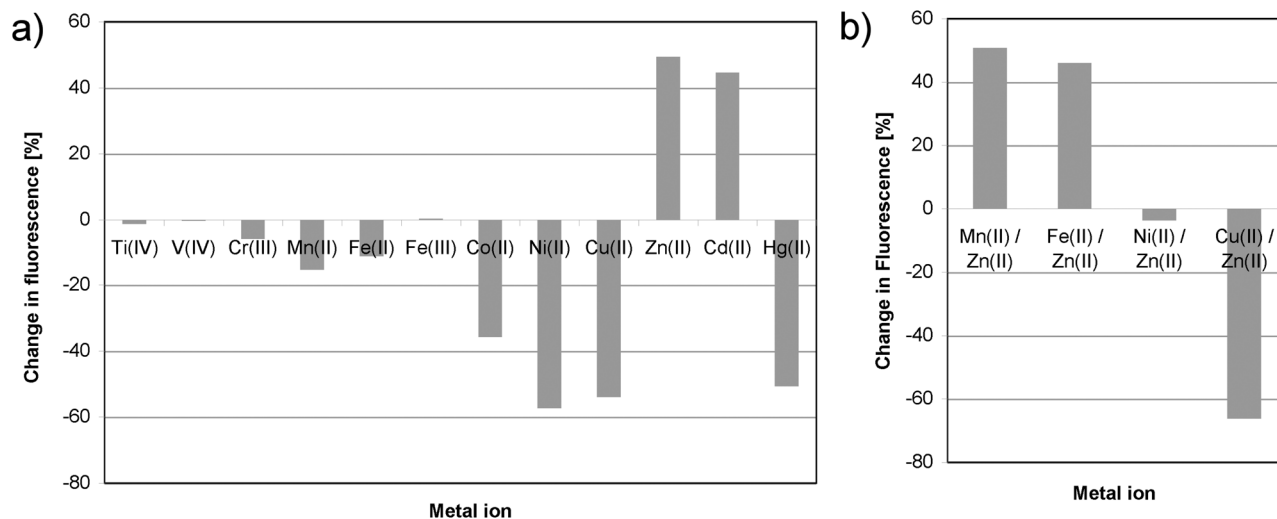
Fig. 6 Change in fluorescence maximum intensity upon (a) addition of one equivalent of metal ions to DMPG vesicles containing 1 mol% of ligand **3**; (b) addition of equimolar mixtures containing one equivalent of Zn^{II} and one equivalent of Mn^{2+}, Fe^{2+}, Ni^{2+} or Cu^{2+} to DMPG vesicles containing 1 mol% of ligand **3**. Conditions: LUV, lipid concentration 0.56 mM, 25 °C, 10 mM phosphate buffer pH = 7.0, total ionic strength 50 mM.

In a second experiment, equimolar mixtures of two different metals were added to check the selectivity for Zn(II) coordination. With Zn^{2+}/Mn^{2+} and Zn^{2+}/Fe^{2+} mixtures a fluorescence *increase* was observed, whereas with Zn^{2+}/Ni^{2+} the fluorescence intensity hardly changed, and with Zn^{2+}/Cu^{2+} a *decrease* was observed (see Fig. 6b). As both Mn^{2+} and Fe^{2+} alone should induce a low decrease of the fluorescence intensity (see Fig. 6a) the data indicate the preferential formation of the Zn(II) complex in such conditions, compared to the Mn(II) or Fe(II) complexes. On the contrary, the strong decrease of the luminescence in the Zn^{2+}/Cu^{2+} mixture shows that coordination of **3** to Cu(II) occurs preferentially compared with Zn(II), which is a known problem of zinc sensors.[19,46,47] Finally, we interpret the low variation of the fluorescence intensity in the Zn^{2+}/Ni^{2+} case as the result of a mixture of Ni(II) and Zn(II) complexes, which may have a similar affinity for the bapbpy manifold.

Discussion and conclusion

In this work, coordination of zinc dichloride was found to turn the water-insoluble bapbpy ligand into a water-soluble, highly fluorescent complex, which was characterized structurally, photophysically, and by DFT calculations. Upon photoexcitation the non-bonded NH bridges of the ligand are able to donate electron density to the central bipyridyl unit. De-excitation is accompanied by photon emission, and the efficiency of this process is enhanced by zinc binding. The recent discovery of the link between zinc metabolism disorders and severe neurological diseases has triggered the search for a new means of measuring free zinc concentration in biological media.[17,21,48–50] Due to the spectroscopically silent nature of Zn(II), fluorescence is the method of choice, and very efficient ligand systems have been published allowing a strong increase

(up to ×150) of the fluorescence upon zinc binding, and high binding constants ($K_a \sim 10^9$ to 10^{12} M^{-1}).[13,18,21,25,51] In order to measure the binding constant of bapbpy to Zn(II) ions in aqueous solution we needed to solubilize the ligand in water. A classical strategy would have been to functionalize it with polar functional groups. However, in order to avoid potential interferences of such groups with the binding strength and/or with the photophysical properties of the zinc complex we considered increasing the lipophilicity of the bapbpy ligand with a neutral alkyl tail, and to insert ligand **3** into liposomes. In the resulting DMPG-based system a modest doubling of the fluorescence intensity upon zinc binding was observed, which is due to the significant fluorescence of the metal-free ligand **3**. The binding constant is too low, too, to measure biologically relevant concentrations of zinc *in vitro*, and competition between Cu(II) and Zn(II) may render such measurements difficult to interpret. For these reasons we did not realize *in vitro* experiments with this system.

In conclusion, although the potential use of unilamellar vesicles in analytical studies has recently been recognized by Giokas and Vlessidis[5] *in vitro* analytical applications are still scarce. In this work we investigated *ex cellulo* the use of liposomes to obtain water solubility of lipophilic metal chelators, and observed the dramatic effect of the charge of the lipid bilayer on the coordination chemistry between the "free" metal cations and the neutral, membrane-embedded ligand **3**. Such electrostatic interactions not only play a role in biology;[3,6,52] they also appear as an essential tuning parameter in the building of liposome-based ion-sensing platforms.

Acknowledgements

References

1 M. Eisenberg, T. Gresalfi, T. Riccio and S. Mclaughlin, *Biochemistry*, 1979, **18**, 5213.

2 B. Klasczyk, V. Knecht, R. Lipowsky and R. Dimova, *Langmuir*, 2010, **26**, 18951.

3 H. Y. Yang, Y. C. Xu, Z. B. Gao, Y. Y. Mao, Y. Du and H. L. Jiang, *J. Phys. Chem. B*, 2010, **114**, 16978.

4 E. Crabb and E. Moore, *Metals and Life*, Royal Society of Chemistry and The Open University, Cambridge, UK, 2010.

5 D. L. Giokas and A. G. Vlessidis, *Anal. Chim. Acta*, 2011, **683**, 156.

6 G. Speelmans, W. H. H. M. Sips, R. J. H. Grisel, R. W. H. M. Staffhorst, A. M. J. Fichtinger-Schepman, J. Reedijk and B. de Kruijff, *Bba-Biomembranes*, 1996, **1283**, 60.

7 G. Speelmans, R W. H. M. Staffhorst, K. Versluis, J. Reedijk and B. de Kruijff, *Biochemistry*, 1997, **36**, 10545.

8 E. C. Constable, W. Meier, C. Nardin and S. Mundwiler, *Chem. Commun.*, 1999, 1483.

9 E. L. Doyle, C. A. Hunter, H. C. Phillips, S. J. Webb and N. H. Williams, *J. Am. Chem. Soc.*, 2003, **125**, 4593.

10 H. Dijkstra, J. Hutchinson, C. Hunter, H. Qin, S. Tomas, S. Webb and N. Williams, *Chem.–Eur. J.*, 2007, **13**, 7215.

11 A. Richard, V. Marchi-Artzner, M. Lalloz, M. Brienne, F. Artzner, T. Gulik-Krzywicki, M. Guedeau-Boudeville and J. Lehn, *Proc. Natl. Acad. Sci. U. S. A.*, 2004, **101**, 15279.

12 J. Voskuhl and B. J. Ravoo, *Chem. Soc. Rev.*, 2009, **38**, 495.

13 B. Gruber, S. Stadlbauer, A. Spaeth, S. Weiss, M. Kalinina and B. Koenig, *Angew. Chem., Int. Ed.*, 2010, **49**, 7125.

14 Z. Arcis Castíllo, S. Zheng, M. A. Siegler, O. Roubeau, S. Bedoui and S. Bonnet, *Chem.–Eur. J.*, 2011, **17**, 14826.

15 S. Bonnet, M. A. Siegler, J. S. Costa, G. Molnar, A. Bousseksou, A. L. Spek, P. Gamez and J. Reedijk, *Chem. Commun.*, 2008, 5619.

16 C. P. Montgomery, B. S. Murray, E. J. New, R. Pal and D. Parker, *Acc. Chem. Res.*, 2009, **42**, 925.

17 K. Kikuchi, K. Komatsu and T. Nagano, *Curr. Opin. Chem. Biol.*, 2004, **8**, 182.

18 E. M. Nolan and S. J. Lippard, *Acc. Chem. Res.*, 2009, **42**, 193.

19 Z. Dai and J. W. Canary, *New J. Chem.*, 2007, **31**, 1708.

20 K. Komatsu, K. Kikuchi, H. Kojima, Y. Urano and T. Nagano, *J. Am. Chem. Soc.*, 2005, **127**, 10197.

21 E. J. New, D. Parker, D. G. Smith and J. W. Walton, *Curr. Opin. Chem. Biol.*, 2010, **14**, 238.

22 K. Jobe, C. H. Brennan, M. Motevalli, S. M. Goldup and M. Watkinson, *Chem. Commun.*, 2011, 1.

23 K. Hanaoka, K. Kikuchi, H. Kojima, Y. Urano and T. Nagano, *Angew. Chem., Int. Ed.*, 2003, **42**, 2996.

24 R. Thompson, *Curr. Opin. Chem. Biol.*, 2005, **9**, 526.

25 N. C. Lim, H. C. Freake and C. Bruckner, *Chem.–Eur. J.*, 2005, **11**, 38.

26 X. L. Bai, X. D. Liu, M. Wang, C. Q. Kang and L. X. Gao, *Synthesis*, 2005, 458.

27 A. J. M. Duisenberg, L. M. J. Kroon-Batenburg and A. M. M. Schreurs, *J. Appl. Crystallogr.*, 2003, **36**, 220.

28 R. Herbst-Irmer and G. M. Sheldrick, *Acta Crystallogr., Sect. B: Struct. Sci.*, 1998, **54**, 443.

29 G. M. Sheldrick, *TWINABS*, University of Göttingen, Germany, 2008.

30 A. Altomare, M. C. Burla, M. Camalli, G. L. Cascarano, C. Giacovazzo, A. Guagliardi, A. G. G. Moliterni, G. Polidori and R. Spagna, *J. Appl. Crystallogr.*, 1999, **32**, 115.

31 G. M. Sheldrick, *Acta Crystallogr., Sect. A: Fundam. Crystallogr.*, 2008, **64**, 112.

32 A. L. Spek, *Acta Crystallogr., Sect. D: Biol. Crystallogr.*, 2009, **65**, 148.

33 M. J. Frisch, G. W. Trucks, H. B. Schlegel, G. E. Scuseria, M. A. Robb, J. R. Cheeseman, J. A. Montgomery, Jr., T. Vreven, K. N. Kudin, J. C. Burant, J. M. Millam, S. S. Iyengar, J. Tomasi, V. Barone, B. Mennucci, M. Cossi, G. Scalmani, N. Rega, G. A. Petersson, H. Nakatsuji, M. Hada, M. Ehara, K. Toyota, R. Fukuda, J. Hasegawa, M. Ishida, T. Nakajima, Y. Honda, O. Kitao, H. Nakai, M. Klene, X. Li, J. E. Knox, H. P. Hratchian, J. B. Cross, C. Adamo, J. Jaramillo, R. Gomperts, R. E. Stratmann, O. Yazyev, A. J. Austin, R. Cammi, C. Pomelli, J. W. Ochterski, P. Y. Ayala, K. Morokuma, G. A. Voth, P. Salvador, J. J. Dannenberg, V. G. Zakrzewski, S. Dapprich, A. D. Daniels, M. C. Strain, O. Farkas, D. K. Malick, A. D. Rabuck, K. Raghavachari, J. B. Foresman, J. V. Ortiz, Q. Cui, A. G. Baboul, S. Clifford, J. Cioslowski, B. B. Stefanov, G. Liu, A. Liashenko, P. Piskorz, I. Komaromi, R. L. Martin, D. J. Fox, T. Keith, M. A. Al-Laham, C. Y. Peng, A. Nanayakkara, M. Challacombe, P. M. W. Gill, B. Johnson, W. Chen, M. W. Wong, C. Gonzalez and J. A. Pople, *GAUSSIAN 03 (Revision D.01)*, Gaussian Inc., Wallingford, CT, 2004.

34 S. Miertus, E. Scrocco and J. Tomasi, *Chem. Phys.*, 1981, **55**, 117.

35 E. J. Bylaska, W. A. de Jong, N. Govind, K. Kowalski, T. P. Straatsma, M. Valiev, D. Wang, E. Apra, T. L. Windus, J. Hammond, P. Nichols, S. Hirata, M. T. Hackler, Y. Zhao, P.-D. Fan, R. J. Harrison, M. Dupuis, D. M. A. Smith, J. Nieplocha, V. Tipparaju, M. Krishnan, Q. Wu, T. Van Voorhis, A. A. Auer, M. Nooijen, E. Brown, G. Cisneros, G. I. Fann, H. Fruchtl, J. Garza, K. Hirao, R. Kendall, J. A. Nichols, K. Tsemekhman, K. Wolinski, J. Anchell, D. Bernholdt, P. Borowski, T. Clark, D. Clerc, H. Dachsel, M. Deegan, K. Dyall, D. Elwood, E. Glendening, M. Gutowski, A. Hess, J. Jaffe, B. Johnson, J. Ju, R. Kobayashi, R. Kutteh, Z. Lin, R. Littlefield, X. Long, B. Meng, T. Nakajima, S. Niu, L. Pollack, M. Rosing,

G. Sandrone, M. Stave, H. Taylor, G. Thomas, J. H. van Lenthe, A. Wong and Z. Zhang, *NWChem, A computational chemistry package for parallel computers, version 5.1*, Pacific Northwest National Laboratory, Richland, Washington 99352-0999, USA, 2007.

36 The CCP1GUI project: http://www.cse.scitech.ac.uk/ccg/software/ccp1gui/ 2008.

37 A. Klamt and G. Schuurmann, *J. Chem. Soc., Perkin Trans. 2*, 1993, 799.

38 M. Mardelli and J. Olmsted, *J. Photochem.*, 1977, **7**, 277.

39 S. Ogawa, N. Kishii and S. Shiraishi, *J. Chem. Soc., Perkin Trans. 1*, 1984, 2023.

40 C. Peltier, P. P. Laine, G. Scalmani, M. J. Frisch, C. Adarno and I. Ciofini, *J. Mol. Struct. THEOCHEM*, 2009, **914**, 94.

41 A. Helle, J. Makitalo, J. Huhtanen, J. M. Holopainen and S. K. Wiedmer, *Biochim. Biophys. Acta, Biomembr.*, 2008, **1778**, 2640.

42 R. Kraayenhof, G. Sterk, H. Wong Fong Sang, K. Krab and R. Epand, *Biochim. Biophys. Acta, Biomembr.*, 1996, **1282**, 293.

43 S. Majee and A. Chakrabarti, *Biochem. Pharmacol.*, 1999, **57**, 981.

44 S. Bonnet, B. Limburg, J. D. Meeldijk, R. J. M. Klein Gebbink and J. A. Killian, *J. Am. Chem. Soc.*, 2011, **133**, 252.

45 T. Kowalczyk, Z. L. Lin and T. Van Voorhis, *J. Phys. Chem. A*, 2010, **114**, 10427.

46 S. C. Burdette, C. J. Frederickson, W. Bu and S. J. Lippard, *J. Am. Chem. Soc.*, 2003, **125**, 1778.

47 J. H. Harvey, S. A. Hilderbrand and S. J. Lippard, *Inorg. Chem.*, 2004, **43**, 2624.

48 S. L. Sensi, P. Paoletti, A. I. Bush and I. Sekler, *Nat. Rev. Neurosci.*, 2009, **10**, 780.

49 P. J. Jiang and Z. J. Guo, *Coord. Chem. Rev.*, 2004, **248**, 205.

50 E. Tomat and S. J. Lippard, *Curr. Opin. Chem. Biol.*, 2010, **14**, 225.

51 S. C. Burdette, C. J. Frederickson, W. M. Bu and S. J. Lippard, *J. Am. Chem. Soc.*, 2003, **125**, 1778.

52 F. Gambinossi, B. Mecheri, G. Caminati, M. Nocentini, M. Puggelli and G. Gabrielli, *Mat. Sci. Eng. C-Biol. Sci.*, 2002, **22**, 283.